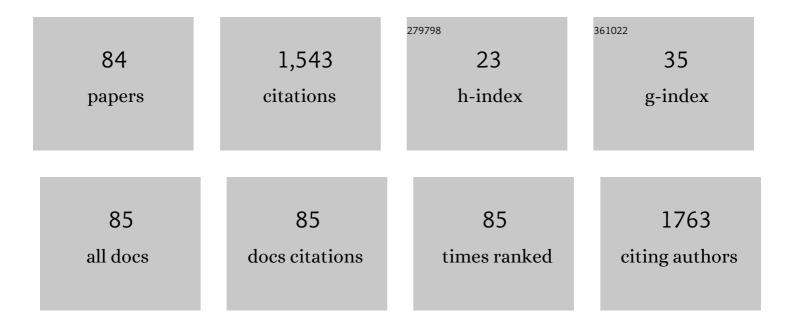


## List of Publications by Year in descending order

Source: https://exaly.com/author-pdf/9828503/publications.pdf

Version: 2024-02-01



#	Article	IF	CITATIONS
1	Coupled substitution of type A and B carbonate in sodium-bearing apatite. Biomaterials, 2007, 28, 916-926.	11.4	198
2	Highâ€ <i>P</i> behavior of anorthite composition and some phase relations of the CaOâ€Al <sub>2</sub> O <sub>3</sub> ‣iO <sub>2</sub> system to the lower mantle of the Earth, and their geophysical implications. Journal of Geophysical Research, 2012, 117, .	3.3	84
3	Formation of abiotic hydrocarbon from reduction of carbonate in subduction zones: Constraints from petrological observation and experimental simulation. Geochimica Et Cosmochimica Acta, 2018, 239, 390-408.	3.9	70
4	The Effects of Small Amounts of H2O, CO2 and Na2O on the Partial Melting of Spinel Lherzolite in the System CaO–MgO–Al2O3–SiO2 ± H2O ± CO2 ± Na2O at 1·1 GPa. Journal of Petrology, 2006, 47	7,2489-434	.52
5	Phase relations in the system KAlSi3O8–NaAlSi3O8 at high pressure–high temperature conditions and their implication for the petrogenesis of lingunite. Earth and Planetary Science Letters, 2006, 246, 317-325.	4.4	46
6	X-ray absorption spectroscopy of ultramarine pigments: A new analytical method for the polysulfide radical anion S3â^ chromophore. Spectrochimica Acta, Part B: Atomic Spectroscopy, 2010, 65, 75-79.	2.9	45
7	The Effect of Cr2O3 on the Partial Melting of Spinel Lherzolite in the System CaO-MgO-Al2O3-SiO2-Cr2O3 at 1{middle dot}1 GPa. Journal of Petrology, 2004, 45, 2261-2286.	2.8	42
8	Accommodation of the carbonate ion in fluorapatite synthesized at high pressure. American Mineralogist, 2008, 93, 1460-1469.	1.9	41
9	Orientation of channel carbonate ions in apatite: Effect of pressure and composition. American Mineralogist, 2011, 96, 1148-1157.	1.9	35
10	Recovery of an oxidized majorite inclusion from Earth's deep asthenosphere. Science Advances, 2017, 3, e1601589.	10.3	33
11	Stability and Reactions of CaCO <sub>3</sub> Polymorphs in the Earth's Deep Mantle. Journal of Geophysical Research: Solid Earth, 2018, 123, 6491-6500.	3.4	32
12	Note: An anvil-preformed gasket system to extend the pressure range for large volume cubic presses. Review of Scientific Instruments, 2010, 81, 116102.	1.3	31
13	Effect of carbon, sulfur and silicon on iron melting at high pressure: Implications for composition and evolution of the planetary terrestrial cores. Geochimica Et Cosmochimica Acta, 2013, 114, 220-233.	3.9	31
14	Equation of state of carbonated hydroxylapatite at ambient temperature up to 10 GPa: Significance of carbonate. American Mineralogist, 2011, 96, 74-80.	1.9	28
15	Raman and infrared spectroscopic quantification of the carbonate concentration in K2CO3 aqueous solutions with water as an internal standard. Geoscience Frontiers, 2021, 12, 1018-1030.	8.4	28
16	Partial Melting of Spinel Lherzolite in the System CaO-MgO-Al2O3-SiO2 Â K2O at 1{middle dot}1 GPa. Journal of Petrology, 2004, 45, 1339-1368.	2.8	27
17	High-pressure study on lead fluorapatite. American Mineralogist, 2008, 93, 1581-1584.	1.9	27
18	Compressibility of a natural kyanite to 17.5GPa. Progress in Natural Science: Materials International,	4.4	25

Xiliii

2009, 19, 1281-1286.

2

Xi Liu

#	Article	IF	CITATIONS
19	Kinetics and Thermodynamics of Mg-Al Disorder in MgAl2O4-Spinel: A Review. Molecules, 2019, 24, 1704.	3.8	25
20	Decomposition of kyanite and solubility of Al2O3 in stishovite at high pressure and high temperature conditions. Physics and Chemistry of Minerals, 2006, 33, 711-721.	0.8	24
21	Thermal expansion of andalusite and sillimanite at ambient pressure: a powder X-ray diffraction study up to 1000°C. Mineralogical Magazine, 2011, 75, 363-374.	1.4	24
22	Equation of state of Â-tricalcium phosphate, Â-Ca3(PO4)2, to lower mantle pressures. American Mineralogist, 2009, 94, 1388-1391.	1.9	23
23	Structural change in lead fluorapatite at high pressure. Physics and Chemistry of Minerals, 2010, 37, 1-9.	0.8	23
24	Type A–B carbonate chlorapatite synthesized at high pressure. Journal of Solid State Chemistry, 2008, 181, 2494-2500.	2.9	22
25	Solid solution between lead fluorapatite and lead fluorvanadate apatite: mixing behavior, Raman feature and thermal expansivity. Physics and Chemistry of Minerals, 2011, 38, 741-752.	0.8	22
26	Fundamental infrared absorption features of α-quartz: An unpolarized single-crystal absorption infrared spectroscopic study. Vibrational Spectroscopy, 2019, 101, 52-63.	2.2	21
27	Carbonated mantle domains at the base of the Earth's transition zone. Chemical Geology, 2018, 478, 69-75.	3.3	20
28	Phase relations of nahcolite and trona at high P-T conditions. Journal of Mineralogical and Petrological Sciences, 2009, 104, 25-36.	0.9	18
29	Thermal expansion of kyanite at ambient pressure: An X-ray powder diffraction study up to 1000°C. Geoscience Frontiers, 2010, 1, 91-97.	8.4	18
30	High-pressure phase relations in the composition of albite NaAlSi3O8 constrained by an ab initio and quasi-harmonic Debye model, and their implications. Earth and Planetary Science Letters, 2010, 298, 427-433.	4.4	18
31	Hydrogen-carbonate ion in synthetic high-pressure apatite. American Mineralogist, 2007, 92, 1764-1767.	1.9	17
32	A large volume cubic press with a pressure-generating capability up to about 10ÂGPa. High Pressure Research, 2012, , 1-16.	1.2	17
33	Solid solutions between lead fluorapatite and lead fluorvanadate apatite: compressibility determined by using a diamond-anvil cell coupled with synchrotron X-ray diffraction. Physics and Chemistry of Minerals, 2012, 39, 219-226.	0.8	16
34	Some thermodynamic properties of larnite (β-Ca <sub>2</sub> SiO <sub>4</sub> ) constrained by high <i>T</i> / <i>P</i> experiment and/or theoretical simulation. American Mineralogist, 2016, 101, 277-288.	1.9	16
35	In situ high-temperature powder X-ray diffraction study on the spinel solid solutions (Mg1â^'x Mn x) Tj ETQq1	1 0.784314	rgBT /Overloc
36	Anhydrous ringwoodites in the mantle transition zone: Their bulkÂmodulus,Âsolid solution behavior, compositional variation, andÂsoundÂvelocity feature. Solid Earth Sciences, 2016, 1, 28-47.	1.7	15

Xı Lıu

#	Article	IF	CITATIONS
37	A first-principles study of the phase transition from Holl-I to Holl-II in the composition KAlSi3O8. American Mineralogist, 2011, 96, 974-982.	1.9	14
38	Compressional behavior of MgCr2O4 spinel from first-principles simulation. Science China Earth Sciences, 2016, 59, 989-996.	5.2	14
39	Si-Disordering in MgAl2O4-Spinel under High P-T Conditions, with Implications for Si-Mg Disorder in Mg2SiO4-Ringwoodite. Minerals (Basel, Switzerland), 2018, 8, 210.	2.0	14
40	The phase boundary between CaSiO3perovskite and Ca2SiO4+ CaSi2O5determined by in situ X-ray observations. Geophysical Research Letters, 2006, 33, n/a-n/a.	4.0	13
41	Expansivity and compressibility of strontium fluorapatite and barium fluorapatite determined by in situ X-ray diffraction at high-T/P conditions: significance of the M-site cations. Physics and Chemistry of Minerals, 2013, 40, 349-360.	0.8	13
42	Pressure-induced phase transition inBaCrO4. Physical Review B, 2010, 81, .	3.2	11
43	Synthetic lead bromapatite: X-ray structure at ambient pressure and compressibility up to about 20ÂGPa. Physics and Chemistry of Minerals, 2011, 38, 397-406.	0.8	11
44	Some IR features of SiO 4 and OH in coesite, and its amorphization and dehydration at ambient pressure. Journal of Asian Earth Sciences, 2017, 148, 315-323.	2.3	11
45	lsotropic Thermal Expansivity and Anisotropic Compressibility of ReB <sub>2</sub> . Chinese Physics Letters, 2011, 28, 036401.	3.3	10
46	Expansivity and compressibility of wadeite-type K2Si4O9 determined by in situ high T/P experiments, and their implication. Physics and Chemistry of Minerals, 2013, 40, 29-40.	0.8	10
47	High-pressure experimental verification of rutile-ilmenite oxybarometer: Implications for the redox state of the subduction zone. Science China Earth Sciences, 2017, 60, 1817-1825.	5.2	10
48	Jianite: Massive Dunite Solely Made of Virtually Pure Forsterite from Ji'an County, Jilin Province, Northeast China. Minerals (Basel, Switzerland), 2020, 10, 220.	2.0	10
49	Thermal elastic behavior of CaSiO3-walstromite: A powder X-ray diffraction study up to 900 ÂC. American Mineralogist, 2012, 97, 262-267.	1.9	9
50	Equation of state of a synthetic ulvöspinel, (Fe1.94Ti0.03)Ti1.00O4.00, at ambient temperature. Physics and Chemistry of Minerals, 2015, 42, 171-177.	0.8	9
51	Spinel and post-spinel phase assemblages in Zn2TiO4: an experimental and theoretical study. Physics and Chemistry of Minerals, 2017, 44, 109-123.	0.8	9
52	Vibrational mode analysis and heat capacity calculation of K2SiSi3O9-wadeite. Physics and Chemistry of Minerals, 2013, 40, 563-574.	0.8	8
53	Non-monotonic compositional dependence of isothermal bulk modulus of the (Mg1–Mn )Cr2O4 spinel solid solutions, and its origin and implication. Solid Earth Sciences, 2016, 1, 89-100.	1.7	8
54	Raman spectroscopic study of synthetic pyrope–grossular garnets: structural implications. Physics and Chemistry of Minerals, 2018, 45, 197-209.	0.8	8

Xi Liu

#	Article	IF	CITATIONS
55	Trace element partitioning between MgAl2O4-spinel and carbonatitic silicate melt from 3 to 6ÂGPa, with emphasis on the role of cation order-disorder. Solid Earth Sciences, 2019, 4, 43-65.	1.7	8
56	High sulfur solubility in subducted sediment melt under both reduced and oxidized conditions: With implications for S recycling in subduction zone settings. Geochimica Et Cosmochimica Acta, 2021, 304, 305-326.	3.9	8
57	Full and ideal mixing behavior between Zr–Wd (K2ZrSi3O9) and Ti–Wd (K2TiSi3O9): evidences from mineral chemistry, X-ray diffraction pattern and Raman spectrum. Physics and Chemistry of Minerals, 2015, 42, 223-234.	0.8	7
58	Thermal equation of state of a natural kyanite up to 8.55 GPa and 1273 K. Matter and Radiation at Extremes, 2016, 1, 269-276.	3.9	7
59	A new Ca3MgSi2O8 compound and some of its thermodynamic properties. Journal of Solid State Chemistry, 2017, 255, 145-149.	2.9	7
60	IR Features of Hydrous Mg2SiO4-Ringwoodite, Unannealed and Annealed at 200–600 °C and 1 atm, with Implications to Hydrogen Defects and Water-Coupled Cation Disorder. Minerals (Basel, Switzerland), 2020, 10, 499.	2.0	7
61	Equation of state of synthetic qandilite Mg2TiO4 at ambient temperature. Physics and Chemistry of Minerals, 2016, 43, 301-306.	0.8	6
62	Equation of State of a Natural Chromian Spinel at Ambient Temperature. Minerals (Basel, Switzerland), 2018, 8, 591.	2.0	6
63	The Study of Crystal Structure on Grossular–Andradite Solid Solution. Minerals (Basel,) Tj ETQq1 1 0.784314	rgBT /Ove 2.0	rlock 10 Tf 50
64	Phase relations and formation of K-bearing Al-10 Ã phase in the MORB+H <sub>2</sub> O system: Implications for H <sub>2</sub> O- and K-cycles in subduction zones. American Mineralogist, 2017, 102, 1922-1933.	1.9	5
65	Water in coesite: Incorporation mechanism and operation condition, solubility and P-T dependence, and contribution to water transport and coesite preservation. Geoscience Frontiers, 2021, 12, 313-326.	8.4	5
66	Thermodynamics of Mg–Al Order-Disorder Reaction in MgAl2O4-Spinel: Constrained by Prolonged Annealing Experiments at 773–1123 K. Molecules, 2021, 26, 872.	3.8	5
67	EFFECTS OF P2O5 AND TiO2 ON THE PARTIAL MELTING OF SPINEL LHERZOLITE IN THE SYSTEM CaO-MgO-Al2O3-SiO2 AT 1.1 GPa. Canadian Mineralogist, 2007, 45, 649-655.	1.0	4
68	MgO partition between olivine and K2O-rich silicate melt: Geothermometers applicable to high potassium magmas. Journal of Asian Earth Sciences, 2018, 166, 181-194.	2.3	4
69	Equations of state of Co2TiO4-Sp, Co2TiO4-CM, and Co2TiO4-CT, and their phase transitions: an experimental and theoretical study. Physics and Chemistry of Minerals, 2019, 46, 571-582.	0.8	4
70	Experimental evidence for a protracted enrichment of tungsten in evolving granitic melts: implications for scheelite mineralization. Mineralium Deposita, 2020, 55, 1299-1306.	4.1	4
71	Compositional characteristics of ringwoodite in the lower part of the mantle transition zone. Solid Earth Sciences, 2020, 5, 223-225.	1.7	4
72	Crystal Structure and Some Thermodynamic Properties of Ca7MgSi4O16-Bredigite. Crystals, 2021, 11, 14.	2.2	4

Xi Liu

#	Article	IF	CITATIONS
73	Quantifying Mg–Al cation distribution in MgAl2O4-spinel using Raman spectroscopy: An experimental calibration. Solid Earth Sciences, 2022, 7, 60-71.	1.7	4
74	High-pressure synthesis, crystal structure and photoluminescence properties of a new terbium silicate: Na <sub>2</sub> Tb <sub>1.08</sub> Ca <sub>2.92</sub> Si <sub>6</sub> O <sub>18</sub> H <sub>0.8</sub> . RSC Advances, 2017, 7, 50195-50199.	3.6	3
75	Effect of second Si–O vibrational overtones/combinations on quantifying water in silicate and silica minerals using infrared spectroscopy, and an experimental method for its removal. Physics and Chemistry of Minerals, 2022, 49, 1.	0.8	3
76	Equation of state of CAS phase to pressure of the uppermost lower mantle at ambient temperature. Science China Earth Sciences, 2011, 54, 1394-1399.	5.2	2
77	A Metastable Fo-III Wedge in Cold Slabs Subducted to the Lower Part of the Mantle Transition Zone: A Hypothesis Based on First-Principles Simulations. Minerals (Basel, Switzerland), 2019, 9, 186.	2.0	2
78	Raman and X-ray diffraction study of pressure-induced phase transition in synthetic Mg2TiO4. Scientific Reports, 2020, 10, 6278.	3.3	2
79	Experimental constraints on trace element partitioning between coesite and hydrous silicate melt at 5 GPa and 1500–1750°C. Science China Earth Sciences, 2021, 64, 1171-1183.	5.2	2
80	Sodium hydrogencarbonate (NaHCO3): coincidence-site lattice twinning and structure refinement. Zeitschrift FÃ1⁄4r Kristallographie, 2009, 224, .	1.1	1
81	Extremely Stable, Highly Conductive Boronâ€Hydrogen Complexes in Forsterite and Olivine. Journal of Geophysical Research: Solid Earth, 2022, 127, .	3.4	1
82	3D-FEM modeling of the microscopic stress field of forsterite aggregate under hydrostatic pressure: Significance of the crystal orientation. Science China Earth Sciences, 2014, 57, 1192-1198.	5.2	0
83	An experimental study of trace element mobility during dehydration of lawsonite blueschist along different P-T paths: Implications for geochemical heterogeneity of Earth's mantle. Journal of Asian Earth Sciences, 2020, 197, 104389.	2.3	0
84	Equation of state of a new calcium magnesium silicate compound with the composition Ca3MgSi2O8 at pressures up to 23 GPa and ambient T. Physics and Chemistry of Minerals, 2022, 49, 1.	0.8	0